Chapter 6

Results

Before experiments on the basically unknown system ClF/Rg were started, the concepts for ultrafast spectroscopy in condensed phase were advanced in the similar and well characterized system I_2/Kr (chapter 2.3.6). Iodine is much heavier than ClF and the dynamics can be measured very accurately to obtain detailed information. This thesis presents the first nearly complete set of pump-probe spectra with systematic variation of pump and probe wavelengths. An evaluation scheme is developed, which allows for interpretation of the experimental data without the aid of simulations. It is transferred to ClF by analogy and results on Cl_2 are reported for completeness.

6.1 Systematic pump-probe spectra on I_2 in Kr

This chapter presents selected results obtained from the fs-pump-probe experiments with systematically varied pump and probe wavelength. The potential diagram is presented in Fig. 6.1 and shows the $X \rightarrow B$ transition (pump), which was tuned from 600 nm to 480 nm, and the $B \rightarrow E$ transition (probe), tuned from 550 nm to 387 nm[1]. Nonradiative relaxation to the states $D'(2_u)$ and δ or

[1] Probe transitions to the f state are not used within this thesis. They can be spectroscopically seperated from transitions to E [115, 116].

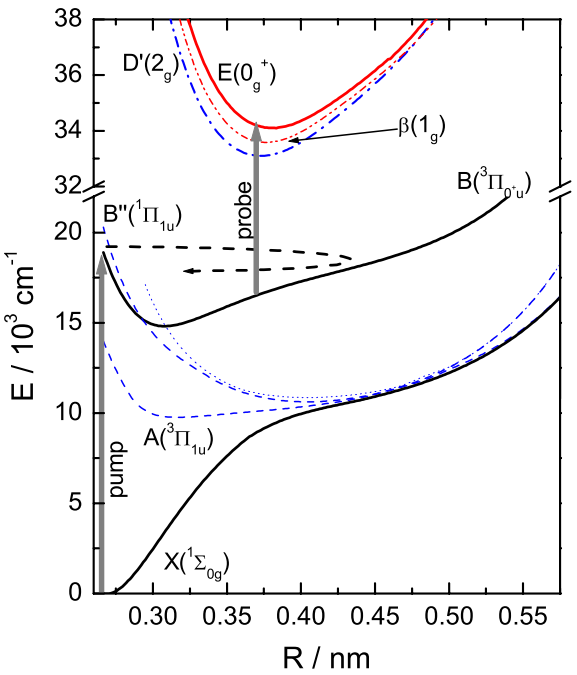

Figure 6.1: Simplified potential diagram for I_2/Kr [204]. The wave function in the ground state X is excited to the B state to create a wave packet (vertical arrow pump). The wave packet is recorded by the probe pulse (vertical arrow probe). After nonradiative relaxation to D' and β, the LIF from these states is detected. The dashed lines indicate the A and B'' states, which can be pumped alternatively. The dotted line indicates the repulsive a state that crosses the B state and causes predissociation [27, 115].

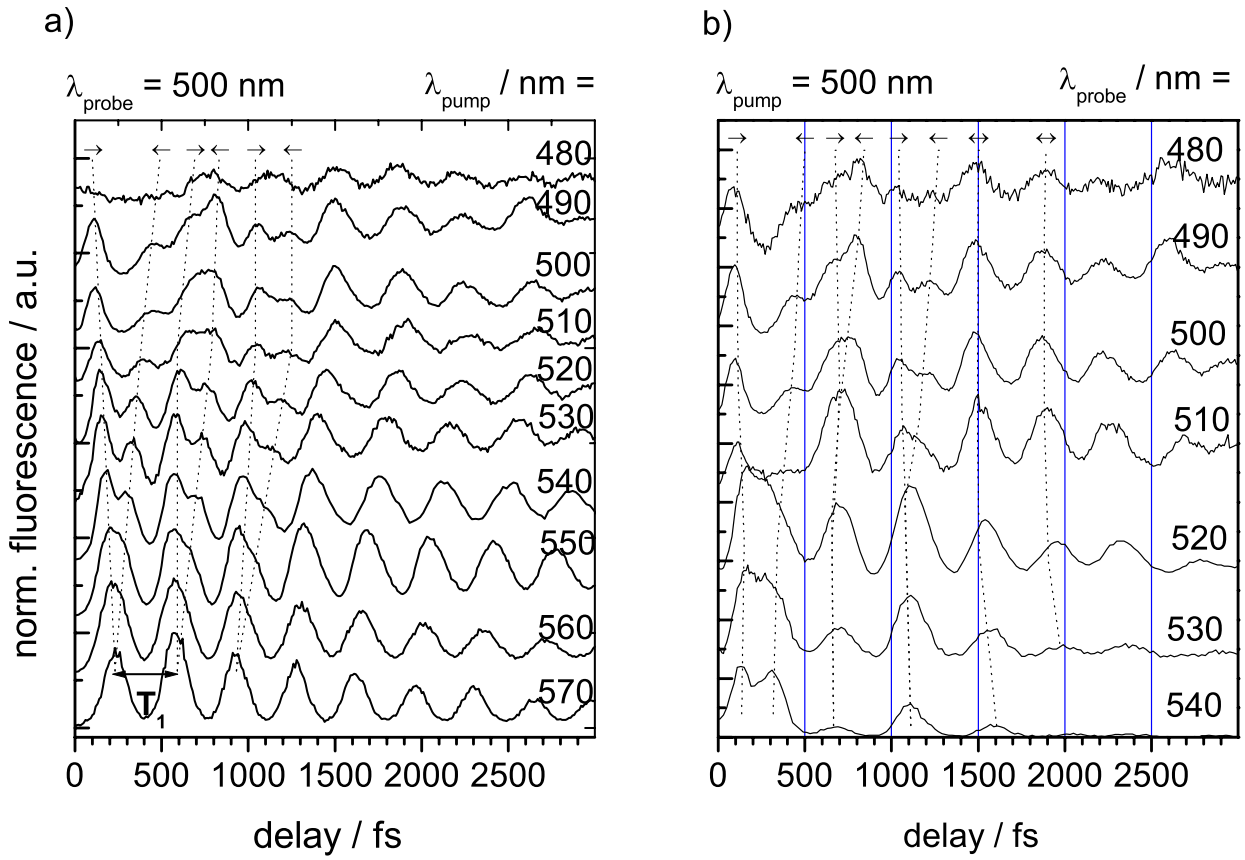

Figure 6.2: Pump-probe spectra for a) $\lambda_{probe} = 500$ nm and $\lambda_{pump} = 570$ to 480 nm and b) $\lambda_{pump} = 500$ and $\lambda_{probe} = 540$ to 480 nm. Dashed lines connect the times for passage through the respective probe windows and the arrows indicate $\rightarrow$ outward and $\leftarrow$ inward motion. T_1 : First round-trip time. Note that strikingly similar trends are observed for variation of a) probe wavelength and b) pump wavelength.

$\beta(1_u)$ results in the recorded LIF signal. The entire collection of the B state spectra is given in the Appendix. These systematic measurements are completed by pump-probe spectra for $A(^3\Pi_1)$ and $B''(^1\Pi_1)$ excitation. All spectra are recorded in I_2/Kr samples with a concentration of $1 : 1000$ at the temperature $T = 15$ K.

6.1.1 Typical B state spectra

Pump-probe spectra for excitation energies which range from deep in the B state well at 570 nm, to the gas phase dissociation limit at 500 nm and even above the dissociation limit (490 and 480 nm) are collected in Fig. 6.2a with a typical probe wavelength $\lambda_{probe} = 500$ nm. For an explanation consider the trace for $\lambda_{probe} = 520$ nm. The thick arrow (pump) in Fig. 6.1 prepares a wave packet on the B state. The first peak in the spectrum corresponds to the first outward passage (dashed arrow) of the wave packet through the probe window (vertical arrow at $R_{win} = 0.376$ nm in Fig. 6.1). The wave packet returns back and passes the probe window a second time, giving rise to the second peak. The periodic motion of the wave packet in the B state potential continues and produces the oscillations in the pump-probe spectrum.

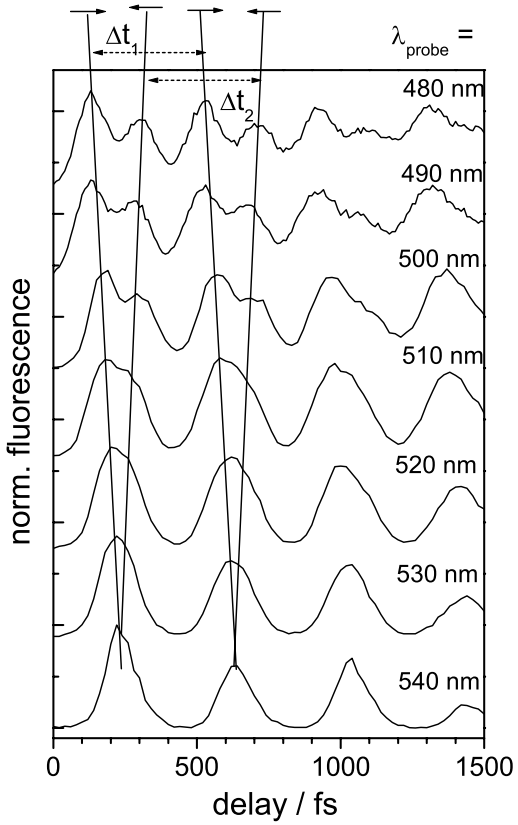

Figure 6.3: Pump-probe spectra with fixed pump wavelength that demonstrate the influence of the probe window. $\lambda_{pump} = 540$ nm: decreasing λ_{probe} from 540 to 480 nm yields an increased splitting between the inward and outward motion of the wave packet indicated by the arrows. The time between two outward passes (Δt_1) and two inward passes (Δt_2) seems to be constant at first sight (cf. Fig 7.3).

In essence, for excitation beyond the probe window the wave packet passes the probe window twice in each complete period, which results in the splitting indicated by the inward and outward pointing arrows in Fig. 6.2a. The wave packet passes the window on the outward motion $(\rightarrow)$ for the first time, on the inward motion $(\leftarrow)$ for the second time and $-$ after one full period $-$ it shows up a third time in the outward and a fourth time on the inward motion. Obviously, one full period corresponds to the time difference between two outward or two inward passes which are connected in Fig. 6.2a by dotted lines as a guide to the eye. For $\lambda_{pump} = 540$ nm the wave packet is excited slightly above the window and the inward/outward splitting occurs for the first time. Qualitatively, it is immediately evident from Fig. 6.2a, that the difference between the first two outward passes indicated by T_1 increases with pump energy E_{pump} as expected by the anharmonicity in a Morse-like potential.

The origin of the inward/outward splitting can be confirmed by tuning λ_{probe} and keeping λ_{pump} fixed at, for example, 540 nm (Fig. 6.3). Taking $\lambda_{probe} = 540$ nm, the wave packet is caught just at the turning point, and the splitting disappears. Shortening λ_{probe} shifts R_{win} inwards, according to the $B - E$ difference potential. For $\lambda_{probe} < 510$ nm the wave packet passes the window twice; it spends a longer and longer time in the region from the window to the outer turning point and back, which results in the increased splitting in Fig. 6.3. Similar trends can be observed for the fixed pump-wavelength $\lambda_{pump} = 500$ nm in Fig. 6.2 b). At this high excitation energy the influence of the matrix is more important and the peak structures are less regular.

In essence, the first complete oscillation period $T_1(E)$ in Fig. 6.2a is the round-trip time of the wave packet at the energy E_{pump}, prepared by the pump pulse. T_1 is taken directly from the spectra and converted to the vibrational frequency $\nu(E) = 1/T_1(E)$, which is plotted in Fig. 7.1.

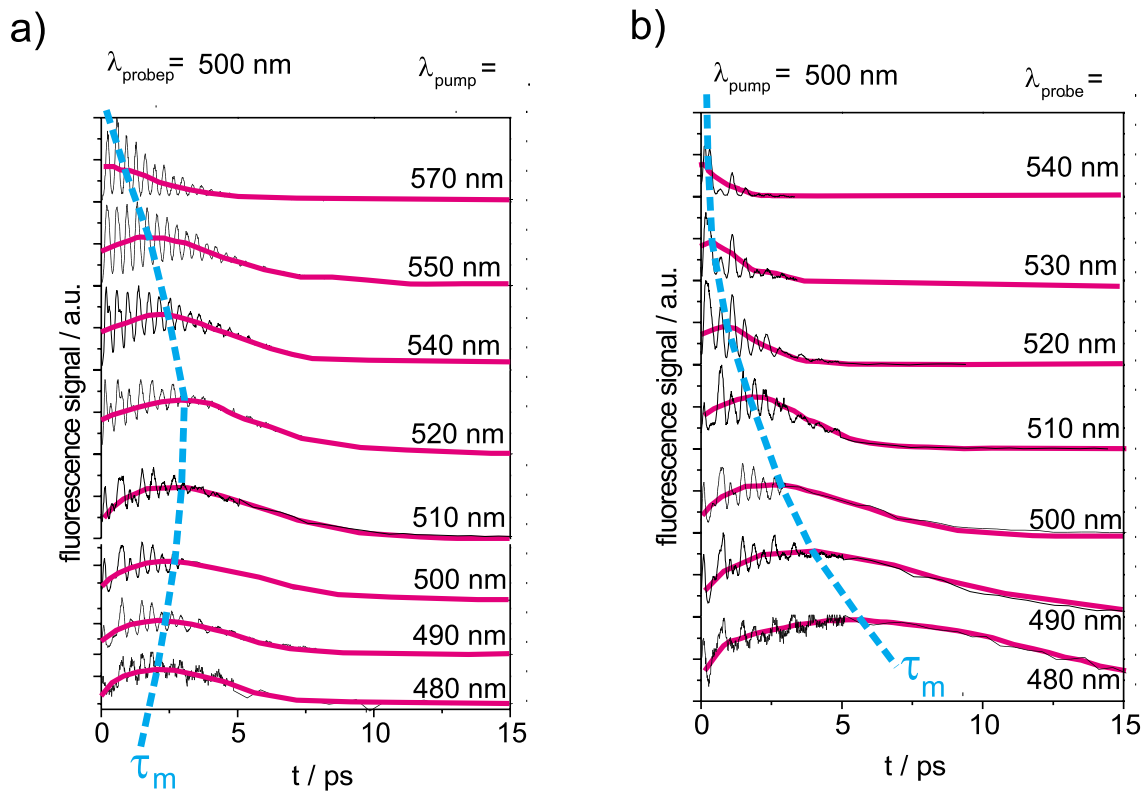

Figure 6.4: Pump-probe spectra from Fig. 6.2 on a stretched timescale. a) $\lambda_{probe} = 500$ nm and $\lambda_{pump} = 570$ to 480 nm and b) $\lambda_{pump} = 500$ and $\lambda_{probe} = 540$ to 480 nm. The dashed lines connect the maxima of the envelopes and indicate τ_m.

Fig. 6.4a shows the spectra from 6.2 on a longer timescale up to 15 ps. The time at which the envelope of the pump-probe spectra is maximal is indicated by τ_m and the dashed line guides the eye. The spectra with fixed $\lambda_{probe} = 500$ nm in panel a) have the longest τ_m for an intermediate pump wavelength $\lambda_{pump} = 520$ nm. Excitation with higher and lower energy leads to a smaller τ_m, i.e. to an earlier maximum of the pump-probe spectrum. For fixed pump wavelengths the time τ_m increases monotonically with decreasing probe wavelength. In chapter 7.4.1 it will be shown that the maximum of the pump-probe envelope occurs, when the vibrational population has relaxed down to the probe window energy E_{win}. The shorter wavelengths probe population deeper in the potential and it takes longer for the wave packet to relax down to this energy. This explains the observed trend in panel b). The explanation for the trend in panel a) lies in the nonlinearly increasing energy dissipation that is displayed in Fig. 7.11 and will be discussed in chapter 7.4.2. The energy dissipation is connected to the loss of coherence (chapter 2.3.3), which smears out the oscillatory structure after several ps in addition to the dispersion effects.

6.1.2 Polarization analysis of pump-probe spectra

Since I_2 occupies a double substitutional site in the Kr lattice and since the size of I atoms is similar to Kr, it is expected that the bond direction will be sterically fixed by the axially symmetric surrounding (sketch of geometry in Fig. 7.15b). This hypothesis excludes depolarization in pump-probe spectra according to the discussion in chapter 2.3.5. The preserved orientation of the molecule is confirmed in the following experiment by changing the relative polarization of the pump and probe pulse.

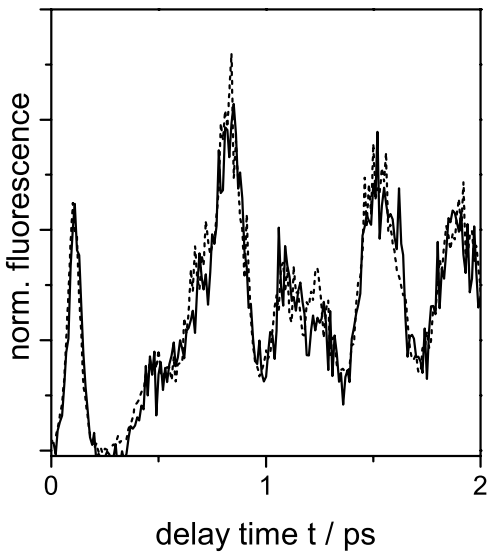

Figure 6.5: Pump-probe spectra with $\lambda_{pump} = 486$ nm and $\lambda_{probe} = 486$ nm for I_2 in Kr. The spectrum for $\parallel$ pump-probe excitation has been multiplied by a factor of 1/3 and agrees perfectly with $\perp$ excitation. The ratio of $I_\perp/I_\parallel = 1/3$ is maintained throughout the entire spectrum, indicating negligible angular reorientation of the I_2 molecule.

Fig 6.5 shows the results for excitation of I_2/Kr above the gas phase dissociation limit[2]. The fluorescence intensity is plotted versus time delay between the pump pulse ($\lambda_{pump} = 486$ nm) and the probe pulse ($\lambda_{probe} = 486$ nm) with probe polarization parallel ($\parallel$) and perpendicular ($\perp$) to the pump. The $\parallel$ - spectrum is multiplied by the factor of $I_\perp/I_\parallel = 1/3$ (cf. Tab 2.3.5) corresponding to preserved photoselection and it shows perfect agreement with the $\perp$ - spectrum. This proves that on the timescale of 2 ps no depolarization, i.e. no reorientation of the molecular bond occurs.

To check the conservation of the initial alignment on a longer timescale, the polarization of the laser induced fluorescence (LIF) from D' after $\parallel$-pump $\parallel$-probe excitation was recorded by introducing a polarization analyzer just in front of the monochromator. Again the ratio for preserved photoselection (cf. Tab. 2.3.5) of $I_{LIF\perp}/I_{LIF\parallel} = 1/5$ is found for LIF polarization $\perp$ / $\parallel$ with respect to the polarization of the pump and probe beams. This indicates that the D' state of I_2 in Kr matrix does not depolarize, i.e. angular reorientation is negligible, on the timescale of the fluorescence lifetime of about 5 ns.

6.1.3 A and B'' state spectra

Fig. 6.6 compares pump-probe spectra for excitation to the A and B'' states. The broken lines display spectra with excitation to the A state with $\lambda_{pump} = 670$ nm and two different probe wavelengths, $\lambda_{probe} = 387$ nm (dashed line) and $\lambda_{probe} = 400$ nm (dotted line)[3]. The first peak ~ 200 fs corresponds to the first outward pass ($\rightarrow$) of the wave packet in the A state through the probe window at $R_{win} \approx 0.38$ nm (Fig. 6.1). The second peak after ~ 1100 fs catches the wave packet on the way back ($\leftarrow$). In the first collision with the Kr matrix, the wave packet has lost so much energy that for all subsequent oscillations the probe window is just reached and the wave packet is only observed once per period ($\leftrightarrow$). The probe wavelength $\lambda_{probe} = 400$ nm is just at the threshold for reaching the ion-pair states according to eq. 2.6. The super-elevated peak at 1.5 ps is a consequence of the response of the Kr lattice. The contracting Kr cage increases the shift of the ion-pair states, moving them into resonance with the probe pulse.

[2]The polarization sensitive pump-probe spectra on I_2/Kr presented in this chapter were taken by Markus Gühr.

[3]The 400 nm beam is the second harmonic of the older Ti:Sa laser system (CPA 1 from Clark), which had a fundamental wavelength around 800 nm.

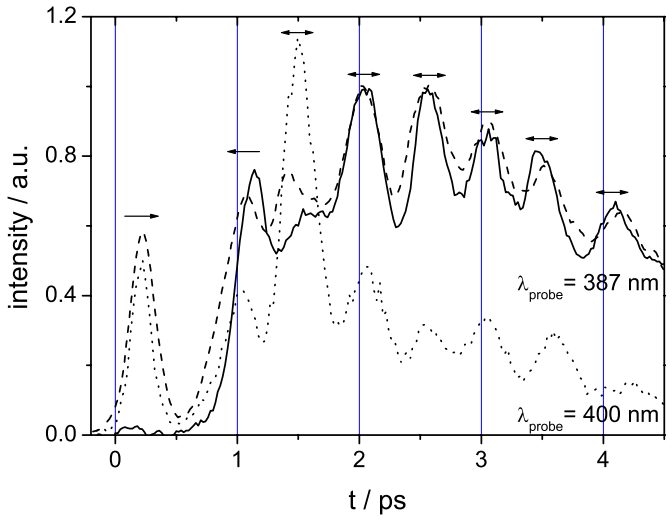

Figure 6.6: Pump-probe spectra on I_2/Kr with a fixed excitation to the A state with a pump wavelength $\lambda_{pump} = 670$ nm and differing probe wavelengths $\lambda_{probe} = 400$ nm (dotted) and 387 nm (dashed). For comparison, the solid line displays excitation to the $^1\Pi_1$ state at $\lambda_{pump} = 480$ nm with $\lambda_{probe} = 387$ nm. Except for the missing peak at 200 fs, this spectrum is almost identical to the A state spectrum recorded with $\lambda_{probe} = 387$ nm. The same effect is seen in the cases of Cl_2/Ar (Fig. 6.17) and ClF/Ar (Fig. 6.11).

The spectrum with $\lambda_{probe} = 387$ nm has a much larger background than the one for $\lambda_{probe} = 400$ nm. The probe window for the shorter wavelength is located deeper in the A state. Thus it probes longer lasting relaxed population than the higher lying probe window (cf. Fig. 2.2). For even shorter probe wavelengths the background keeps increasing [29]. This is equivalent to the signals for B state excitation (Fig. 6.4b).

The solid line in Fig 6.6 shows a spectrum for excitation to the $B''(^1\Pi_1)$ state, recorded with $\lambda_{probe} = 387$ nm, as well. It is generated with $\lambda_{pump} = 480$ nm (solid line), while the $A^3\Pi_1$ state is prepared with $\lambda_{pump} = 670$ nm (dashed line). The spectra are nearly identical after 1 ps, demonstrating that the B'' population nonadiabatically relaxes down to the A state during this time. The higher excess energy is quickly dissipated in the first ps. The main difference of the two spectra is the peak at 200 fs, which is not present for $B''(^1\Pi_1)$ excitation, since there is no probe window in that state. The crossing to the A state occurs at large R in the first round-trip, analogous to the case of ClF/Ar and Cl_2/Ar.

6.2 Road map for condensed phase pump-probe spectra

From the preceding chapter, together with all other pump-probe spectra on I_2/Kr that are collected in the Appendix, a compact diagram can be distilled. It is a useful road map for pump-probe spectra of diatomics in the condensed phase in general and will prove helpful in the discussion of ClF and Cl_2 spectra. In this sense I_2/Kr can be used as a model system to guide the experiments and the interpretation of the pump-probe spectra on similar systems that are less well understood. The diatomics, that are the topic of the present thesis, all have qualitatively similar potentials. The final state of the probe transition has a larger equilibrium distance than the state where the dynamics take place.

Fig. 6.7a shows a typical potential diagram. The wave function in the ground state X is promoted to the excited B state, creating a wave packet in the vibrational levels around the energy $E_{pump.}$ The outer turning point is indicated as $R_{pump.}$ The probe pulse defines the probe window location R_{win} to the E state by the resonance condition $\hbar\omega_{probe} = \Delta V(R_{win})$. The minimum $R_{\min \Delta V}$ of the difference potential $\Delta V = E_E - E_B$ is often quite close to the minimum of the final E state.

Fig. 6.7b) is a diagram summarizing the properties of pump-probe spectra as a function of λ_{pump} on the vertical axis (energy in excited state) and of λ_{probe} on the horizontal axis, defining the location of the probe window R_{win}. The highest possible pump wavelength (640 nm for I_2) is defined by the minimum T_e of the B state. The corresponding probe window (387 nm) lies on the left border of

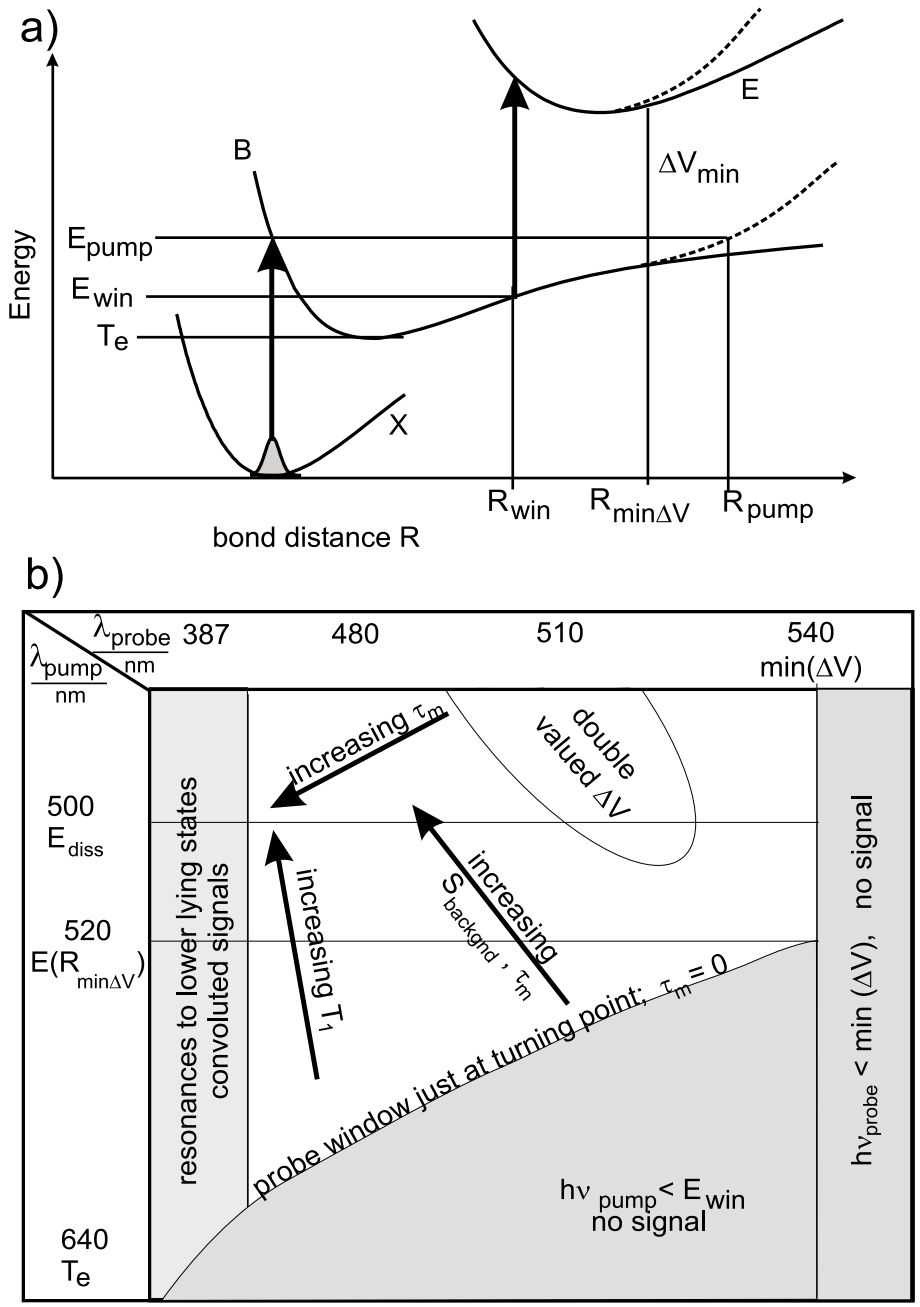

Figure 6.7: a) Schematic potential energy diagram for diatomics in condensed phase with the notation introduced in Fig. 2.9. b) Road map for the systematic set of pump-probe spectra for the B state of I_2/Kr (see Appendix) summarizing the observed trends. The pump wavelength is indicated vertically since it specifies the energy of the wave packet. The probe wavelength is varied on the horizontal axis, as this corresponds to a variation of the probe window (cf. panel a). In the light grey region the signal is a convolution with lower lying electronic states. In the dark grey region, no signal can be observed, and at its border the probe window R_{win} is just at the turning point R_{pump}. The arrows indicate trends in the pump-probe spectra when pump and probe wavelengths are tuned. T_1 is the first oscillatory period, τ_m is the maximum of the envelope and $S_{backgnd}$ indicates the background from smeared out oscillations.

the diagram, although in general, shorter probe wavelengths are possible for probing the inner limb of the B state. At shorter wavelengths, however, resonances to lower potential energy surfaces (e.g. A state) start to play a role and the pump-probe spectra are a convolution of contributions from both states, which is indicated by the light-grey shaded area. The right border of the diagram is given by the minimum of the difference potential. For $\lambda_{probe} < \min(\Delta V)$ (540 nm) no signal is observed. This is marked by the dark grey shaded area, as well as the region where $h\nu_{pump} < E_{win}$. At the borderline of the dark area, the probe window R_{win} is just at the turning point R_{pump}. The condition $E_E(R_{pump}) = h\nu_{pump} + h\nu_{probe}$ is fulfilled, which will be used in chapter 7.1.3 to construct the E state from the systematic spectra. Above the horizontal line for $E(R_{\min \Delta V})$ (520 nm) the wave packet can access two probe windows to the E state, since the difference potential is double-valued. However, the region in which the outer window is observed, is limited since the probe wavelength must not be too short.

The arrows indicate the trends observed in pump-probe spectra. The first period T_1 increases with decreasing pump wavelength and slightly with decreasing probe wavelength. The background signal $S_{backgnd}$ from relaxed and dephased population increases, together with the time τ_m for the maximum of the pump-probe envelope, with decreasing λ_{pump} and $\lambda_{probe.}$ Near the gas phase dissociation limit E_{diss} (500 nm) and upwards, this trend continues for $S_{backgnd}$, but here τ_m is reduced with higher pump energy due to the nonlinear dissipation of energy (cf. Fig. 6.4 and chapter 7.4.2).

6.3 Pump-probe spectra for ClF in Ar and Kr

The bleaching experiments for ClF in Ar and Kr demonstrated, that the dissociation quantum efficiency in Ar is low ($\sim$ 5 %), while in Kr it is very large ($\sim$ 50 %) (chapter 5.4.1). In Ar the fluorescence of Cl^+F^- at $\lambda_{LIF} = 420$ nm was identified (Fig. 4.5), and probing to these ion-pair states can be used to monitor the recombination dynamics of ClF. In Kr this fluorescence is missing but instead the dominant fluorescence originates from $Kr_2^+F^-$ at $\lambda_{LIF} = 460$ nm (Fig. 4.6), which can be used to monitor the F fragments after ClF dissociation.

6.3.1 B state excitation

ClF/Ar is excited to the B state above the dissociation limit, since the focus of this study is on dissociation-recombination dynamics and on strong interaction of the molecule with the solvent. The spectra are recorded with the fixed pump wavelength of the second harmonic of the Ti:Sa at $\lambda_{pump} = 387$ nm, i.e. 0.6 eV above the gas phase dissociation limit[4]. This is the maximum of the B state absorption. The location of the probe window R_{win} is varied by scanning the probe wavelength. This corresponds to a horizontal line in the "Road map of condensed phase pump-probe spectroscopy" (Fig. 6.7).

Overview and envelope

The pump-probe spectra for ClF/Ar are recorded in the same scheme as for I_2/Kr. The femtosecond pump pulse at $\lambda_{pump} = 387$ nm prepares a vibrational wave packet on the weakly bound B ($^3\Pi_0$)-state above the gas-phase dissociation limit (Fig. 4.1). A probe pulse with $\lambda_{probe} < 322$ nm promotes the population to the ionic E state in the Cl^+F^- manifold (cf. chapter 4.2.1). This is indicated by the solid arrow $h\nu_1$ in Fig. 4.1. After relaxation within the Cl^+F^- ionic manifold the fluorescence from the lowest state, D', is observed (Fig. 4.5) [205]. The signal intensity is recorded as a function of time delay between the two pulses. Fig. 6.8 shows pump-probe spectra with systematic variation of the probe wavelengths from 322 to 282 nm, keeping the pump wavelength fixed at $\lambda_{pump} = 387$ nm.

For $\lambda_{probe} > 322$ nm the probe resonance is lost. Hence this wavelength corresponds to the minimum of the difference potential $\Delta V = V_E - V_B$ between the B and the E state (chapter 2.3.2).

[4] In the present setup the laser cannot be spectrally tuned in this wavelength region.

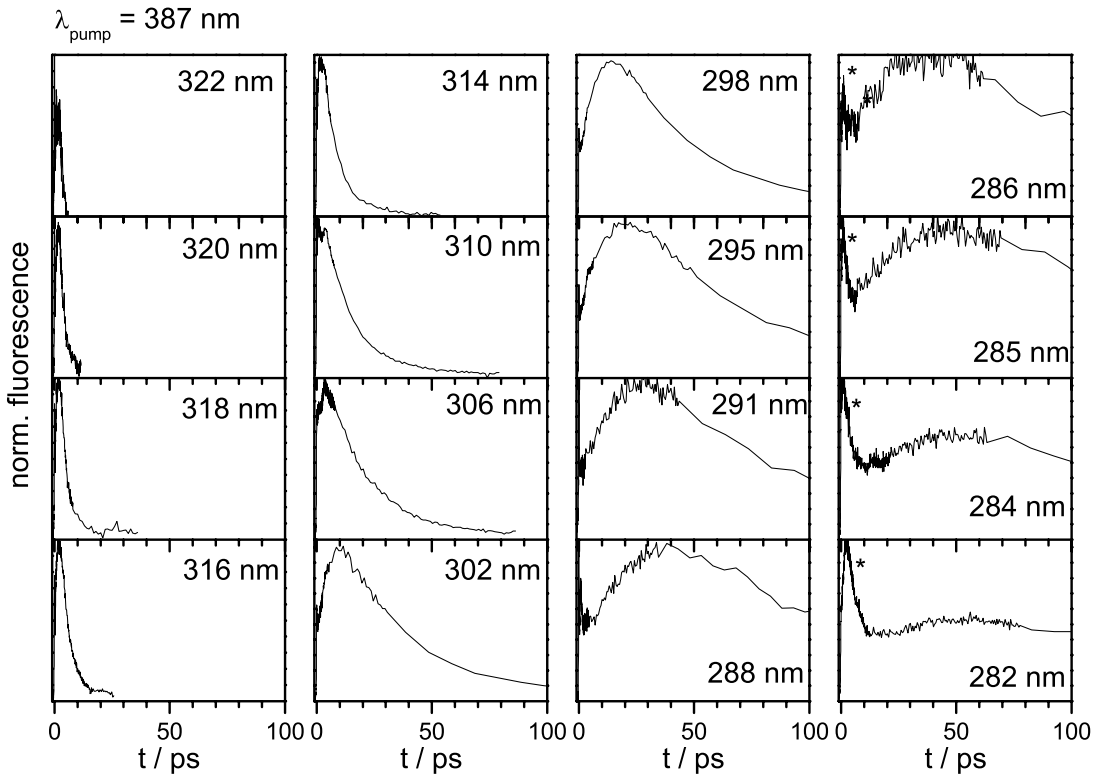

Figure 6.8: Pump-probe spectra with $\lambda_{pump} = 387$ nm, where λ_{probe} is varied from 322 to 282 nm. The fluorescence is detected at $\lambda_{LIF} = 420$ nm. Therefore ClF and Cl_2 population is observed (cf. Fig. 4.8). The maxima of the pump-probe envelope correspond to the delay time τ_m at which the vibrational population of ClF passes E_{win} (see Tab. 7.3). The early maxima in the last column, marked with an asterisk (*), correspond to Cl_2 as discussed in chapter 6.4. The assignment of the latter dynamics to Cl_2 was tested by preparation of pure Cl_2/Ar samples without ClF impurities. Consistently, the ClF contributions are then absent (cf. Fig 6.15).

The shifted difference potential ΔV of ClF in Ar matrix (Fig. 5.6) is derived from this value. The same trend as for I_2/Kr is observed when tuning the probe wavelength. Shorter wavelengths probe deeper parts of the B state potential and the maximum of the envelope τ_m shifts to later times. A more detailed examination of the envelopes for $\lambda_{probe} = 314$ to 306 nm shows the presence of two maxima, which are due to absorptions to two different states, E and f, respectively (cf. Fig. 5.6). The interpretation of spectra with $\lambda_{probe} > 310$ nm is more straight forward, since only the E state resonance can be reached.

For $\lambda_{probe} < 288$ nm an additional maximum near $t = 0$ marked with an asterisk (*) appears, which is due to the Cl_2 molecules present in the sample. The spectra are shown and discussed below.

Oscillations

Fig. 6.9 displays on an enlarged scale the first 3 ps of pump-probe signals of ClF/Ar for the first three rows from Fig. 6.8. In the first row, the probe pulse terminates only in the E state and those spectra show oscillations in the first 1.5 ps due to several passes of the wave packet through the probe window. All other spectra have the early peak near $t = 40$ fs in common, which can be attributed to the first passage of the wave packet through the probe window. The last two spectra for $\lambda_{probe} = 291$ and 288 nm represent a superposition of ClF and Cl_2 contributions, which results in the super-elevated early maximum. The deconvolution is discussed in chapter 7.8. Again, as for I_2/Kr it is evident that the modulation depth decreases on probing deeper in the potential well and hence no oscillations could be detected for $\lambda_{probe} < 314$ nm. The assignment of the oscillations will be given in chapter 7.3.2, after the dynamics of the analog model system I_2/Kr has exemplified the peak-structure.

6.3.2 Polarization dependent pump-probe spectra

ClF/Ar, excited above the gas phase dissociation limit, shows a significant depolarization in contrast to the sterically fixed I_2/Kr. The emission from D' (50 ns lifetime) after $\|$-pump $\|$-probe excitation is completely depolarized, i.e. the fluorescence is isotropic and unpolarized. Therefore, the direction of the fluorescence detection is irrelevant and a $90°$ configuration is chosen to reduce the stray light. In order to observe reorientation on the timescale of the wave packet dynamics, the probe wavelength should be long, since short probe wavelengths delay the highest sensitivity τ_m to later times (cf. Fig 6.8). Fig. 6.10 shows spectra ($\lambda_{pump} = 387$ nm and $\lambda_{probe} = 317$ nm) with parallel ($\|$ solid line) and perpendicular ($\perp$ dotted line) pump-probe polarization, as well as pump-probe polarization close to the magic angle (dashed), all on the same intensity scale.

The magic angle configuration produces a spectrum intermediate between parallel and crossed polarization. It is insensitive to angular dynamics by definition of the magic angle and will therefore be used to characterize the vibrational wave packet dynamics in chapter 7.3.2. The parallel and magic angle spectra both show a pronounced dip at 300 fs, which will be attributed in part to breathing motion of the cage in chapter 7.3.2. In the perpendicular ($\perp$) configuration, a broad minimum with a small maximum is observed after 300 fs. The $\perp$ polarization is sensitive especially to molecules that are tilted 90° with respect to the pump geometry and this suggests that this peak is due to scattering events that produce this geometry after the first encounter. All signals coincide for delay times longer than 2 ps, indicating that the anisotropy prepared by the pump pulse decays on this timescale.

In ClF/Ar nonradiative relaxation to A' is fast and the only observed $A' \rightarrow X$ emission has a lifetime of 141 ms. It is completely depolarized after excitation with 387 nm since it is a $\Delta\Omega = 2$ transition and in addition the orientation of the molecule is randomized within 1.2 ps. This was tested by introducing a polarization analyzer as discussed in chapter 6.1.2.

6.3.3 $^1\Pi$ state excitation

Pump wavelengths in the range from 310 to 260 nm excite ClF/Ar to the repulsive $^1\Pi$ state. Spectra for three different probe wavelengths between 318 and 302 nm are plotted in Fig. 6.11 as dashed

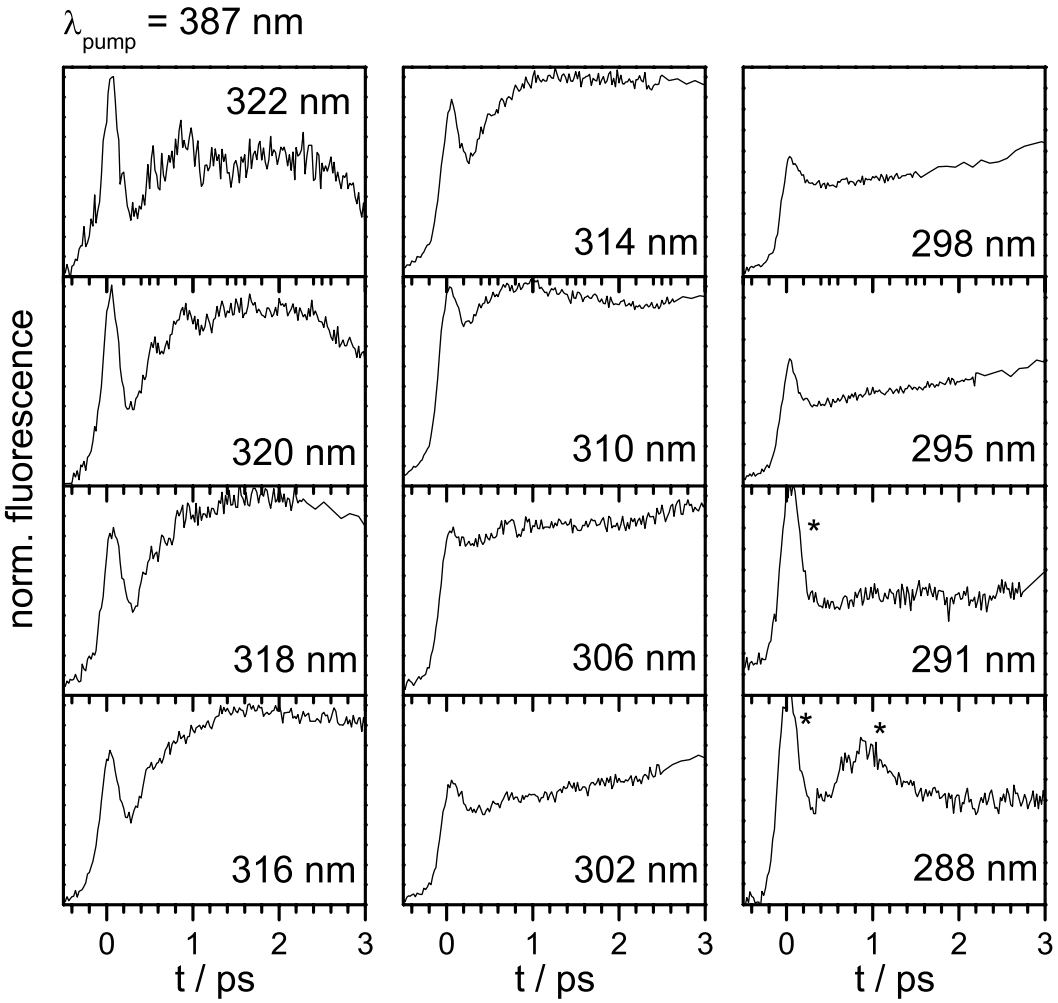

Figure 6.9: Pump-probe spectra with $\lambda_{pump} = 387$ nm and probe wavelength tuned from $\lambda_{probe} = 322$ to 288 nm. Wave packet dynamics are clearly visible in the first column with the longest probe wavelengths. The minimum at 200 fs becomes more and more substantial with increasing wavelengths (see text). The asterisk (*) in the last two plots ($\lambda_{probe} = 291$ and 288 nm) indicates contributions from Cl_2.

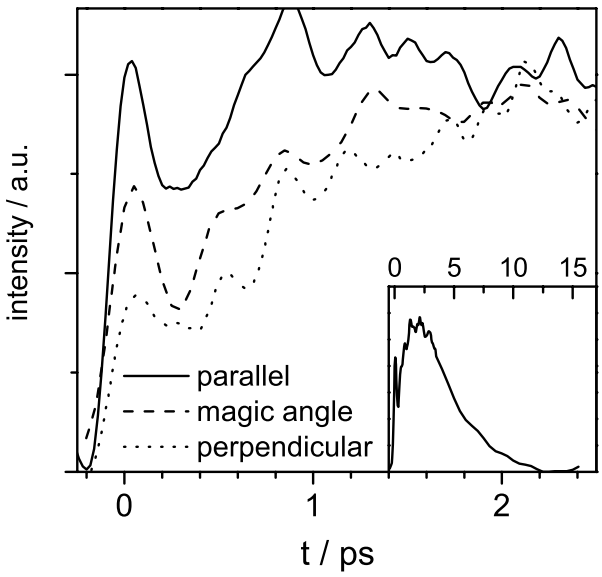

Figure 6.10: fs-pump-probe spectra with $\lambda_{pump} = 387$ nm and $\lambda_{probe} = 317$ nm for ClF in Ar for $\parallel$, $\perp$ and magic angle configuration of pump and probe polarization. The spectra converge after 2 ps, demonstrating the ultrafast randomization of the initially prepared alignment. The inset displays the spectrum on a longer timescale.

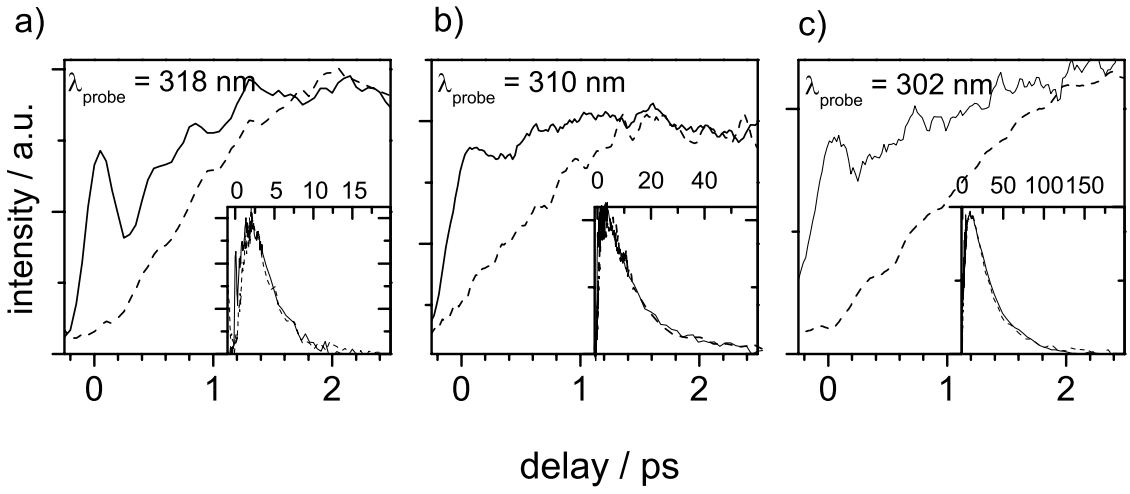

Figure 6.11: Pump-probe spectra that compare singlet excitation (dashed) to triplet excitation (solid). The $B(^3\Pi_0)$ state is pumped with $\lambda_{pump} = 387$ nm and $^1\Pi_1$ state with $\lambda_{pump} = 280$ nm for panel a) and 290 nm for panels b) and c). Three different wavelengths probe the wave packet at different energies a) $\lambda_{probe} = 318$ nm, b) $\lambda_{probe} = 310$ nm and c) $\lambda_{probe} = 302$ nm. All spectra show oscillations due to wave packet dynamics. Note the different timescales in the insets.

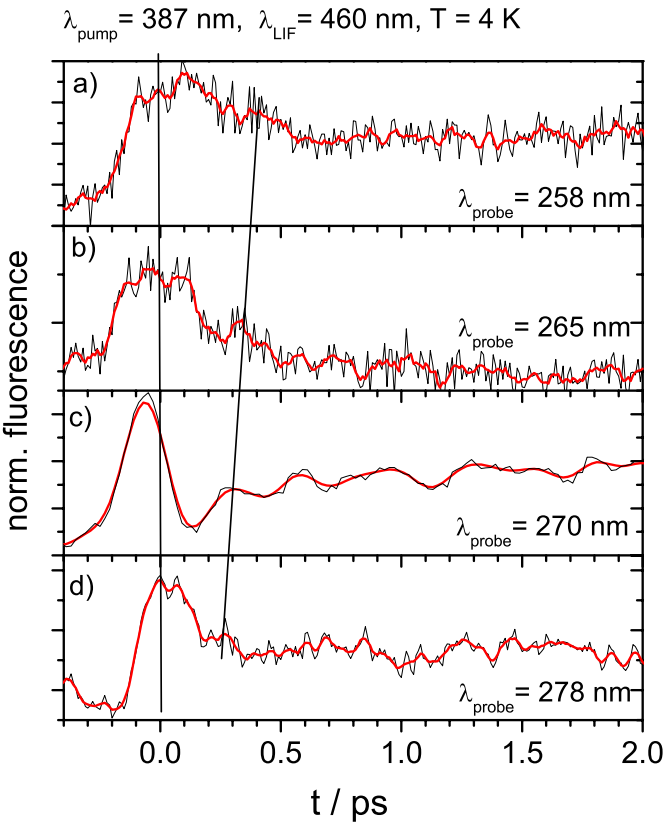

Figure 6.12: Pump-probe spectra on ClF/Kr samples at 4 K with $\lambda_{pump} = 387$ nm and LIF from $Kr_2^+F^-$ recorded at $\lambda_{LIF} = 460$nm. The probe wavelength λ_{probe} is varied: a) 258 nm, b) 265 nm, c) 270 nm and d) 278 nm. The vertical line indicates $t = 0$ and the second line guides the eye to the first maximum around $t = 0.3$ ps.

lines. For the first 2 ps, the signals differ significantly from those after excitation to the $B(^3\Pi_0)$ state at 387 nm. For longer times they coincide perfectly, after normalization to the same intensities, which accounts for the different absorption cross section and photon flux. Shorter probe wavelengths record the B state population with lower vibrational excitation (see above) and the signal can be observed up to 100 ps. For these probe wavelengths, the only allowed transition that are accessible are from $^3\Pi_\Omega$ states to the states with the same quantum numbers in the ionic manifold. All these transitions have difference potentials very close to the $B \rightarrow E$ transition, and a separation seems impossible (Fig. 5.6). That the spectra in Fig. 6.11 agree for times $t > 2$ ps immediately implies, that the molecule nonadiabatically decays from the initially excited $^1\Pi$ state to the bound $^3\Pi$ states on this ultrafast timescale. This surprising result will be further analyzed in chapter 7.6. If the population was transferred to the repulsive $^3\Pi$ states, there should also be a signal for $\lambda_{probe} > 322$ nm, according to the difference potential in Fig. 5.6. This resonance could not be observed up to now.

The signal envelope (insets) of the signals for $^1\Pi$ excitation shows the signature of vibrational relaxation, already observed above for the B state and described in chapter 6.2. First, the signal increases as the wave-packet relaxes into the probe window, improving the Franck-Condon overlap with the ionic states. Then as the wave packet loses energy, it is unable to reach the probe window and the signal decreases towards zero.

6.3.4 Pump-probe spectra with $Kr_2^+F^-$ fluorescence

The F fragments are monitored after ClF dissociation in ClF/Kr samples. The pump-probe spectra presented in this chapter use $\lambda_{pump} = 387$ nm, i.e. $B(^3\Pi_0)$ excitation. The detected fluorescence $\lambda_{LIF} = 460$ nm is indicative of the formation of the $Kr_2^+F^-$ exciplex, as it was shown in chapter 5.2.2. Two different regimes must be distinguished for the probe wavelength. If $\lambda_{probe} < 278$ nm,

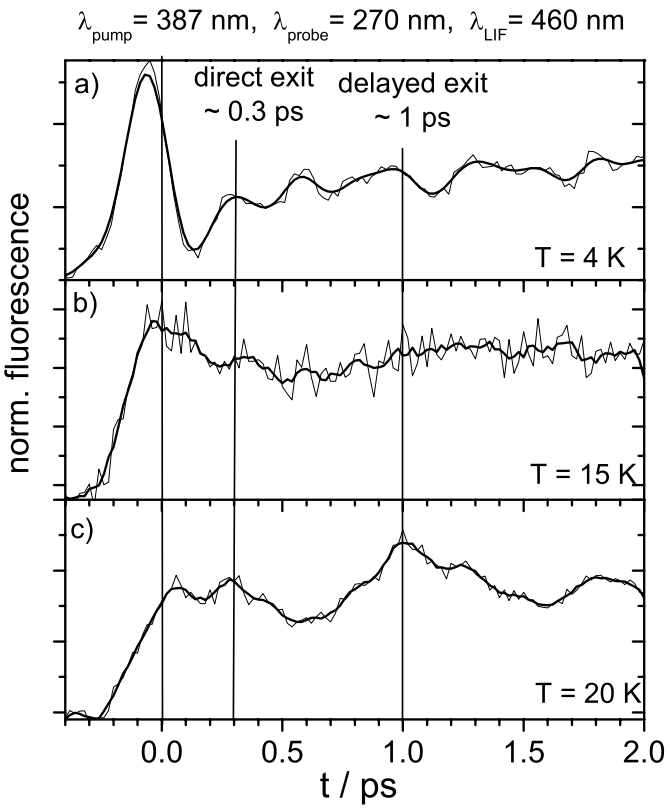

Figure 6.13: Pump-probe spectra with on ClF/Kr samples with $\lambda_{pump} = 387$ nm, $\lambda_{probe} = 270$ nm and LIF from $Kr_2^+F^-$ recorded at $\lambda_{LIF} = 460$ nm. The temperature is varied: a) 4 K (F fragments frozen), b) 15 K (threshold for F mobility) and c) 20 K (F thermally mobile).

besides the escaping F atoms also the isolated cold F atoms in the Kr lattice are probed as in the static experiments. For this reason, the "lock-in" technique (Appendix) was applied that subtracts this static background and only yields contributions from F atoms that have just been excited. For $\lambda_{probe} > 278$ nm this static background is not present and the pump-probe spectra are recorded as usual.

Fig. 6.12 shows spectra recorded at 4 K with a variation of probe wavelength from $\lambda_{probe} = 278$ nm to 258 nm. Care was taken to accurately measure the zero time delay $t = 0$ by the FROG technique. The best signal to noise ratio is obtained for probing at 270 nm, which is the maximum of the KrF absorption at 4 K and for small irradiation doses (Fig. 4.9). Clearly reproducible features in all spectra are the maximum at negative delay times (approx. -50 fs) and the peak at ~ 300 fs, marked by a line to guide the eye. The exact time t_1, where the peak occurs, depends on the probe wavelength and varies from $t_1 \sim 250$ fs for $\lambda_{probe} = 278$ nm to $t_1 \sim 350$ fs for $\lambda_{probe} = 258$ nm. Since the cage exit probability for ClF in Kr is very high, the concentration of ClF quickly decays (cf. Fig. 4.12). A compromise has to be found concerning the number of pulses used for averaging and the bleaching rate. Most of the spectra are averaged over 500 to 1000 shots per point. For longer averaging the structures observed in the spectra are reduced due to the decaying ClF content. Several runs with 500 to 1000 shots on fresh sample positions are averaged to yield the plotted spectra. The peak at negative time delays, which is most clearly seen in the spectrum for $\lambda_{probe} = 270$ nm, depends quadratically on the intensity I_{387} of the pump pulse ($\lambda_{pump} = 387$ nm), while the spectrum for positive time delay scales linearly with intensity. I_{387} was reduced as much as possible to minimize the contribution at $t = -50$ fs. The bleaching weakens all structures in a similar manner, indicating that they originate from nascent ClF fragments.

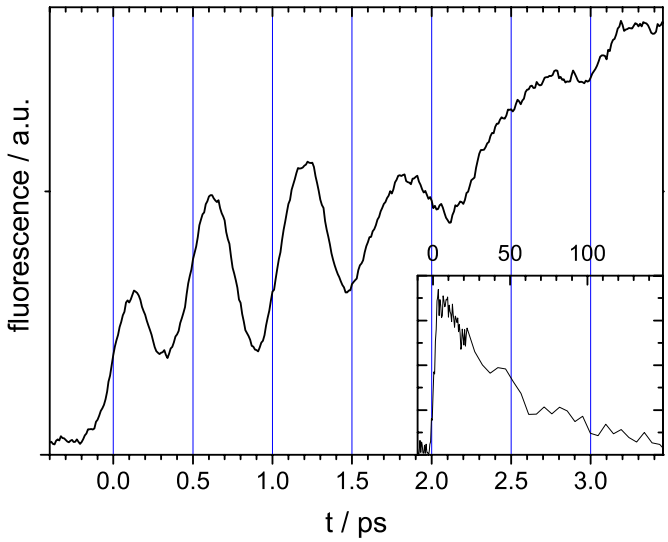

Figure 6.14: Pump-probe spectrum recorded in ClF/Kr samples at 20 K with $\lambda_{pump} = 387$ nm and $\lambda_{probe} = 289$ nm. The fluorescence band that shows the oscillations is centered at $\lambda_{LIF} = 480$ nm with a width of 50 nm and is thus identified as the $Kr_2^+F^-$ fluorescence. In chapter 7.7.3 this will be ascribed to cage dynamics of the Kr lattice around an F fragment.

Fig. 6.13 shows spectra for three different temperatures, $T = 4$, 15 and 20 K, recorded with the probe wavelength $\lambda_{probe} = 270$ nm, which provides the best signal to noise ratio. The peak ~ 300 fs is present in all spectra and the broad feature after 1ps is dominant especially in warm matrices ($T = 20$ K). In Kr the F fragments become mobile at $T = 15$ K. Note that in warm matrices ($T = 20$ K) the thermal motion of F fragments leads to recombination, which changes the bleaching of ClF. Moreover, the F atoms migrate out of the laser focus.

Fig. 6.14 shows a spectrum recorded with $\lambda_{probe} = 289$ nm at the temperature $T = 20$ K. The "lock-in" technique is not needed, since the cold trapped F radicals are not probed at this long wavelength; however, it yields identical results. The spectrum shows very well modulated oscillations. The oscillation period in Fig. 6.14 increases from 550 fs in the beginning to 750 fs around 2.5 ps. The fluorescence in the minima and maxima of the oscillation was measured, to confirm that the deep modulation really corresponds to a coherent motion of F atoms. The fluorescence band that identifies the oscillating species was recorded by subtracting the fluorescence in the second minimum at 900 fs from the one on the second maximum around 650 fs. The resulting band is centered at 480 nm with 50 nm bandwidth. It agrees with the $Kr_2^+F^-$ fluorescence (cf. Fig. 4.6) and thus the oscillations indeed originate from F fragments.

The longest wavelength, that produces a fluorescence signal at $\lambda_{LIF} = 440$ to 510 nm in pump-probe spectra corresponds to $\lambda_{probe} = 310$ nm. All spectra for λ_{probe} between 310 and 278 nm show structures similar to Fig. 6.14 or Fig. 6.13.

6.4 Pump-probe spectra on Cl_2 in Ar

This chapter gives a short account of the new results obtained for Cl_2/Ar, which represent the first ultrafast pump-probe spectra of this molecule. The experiments were necessary to separate the Cl_2 contribution from the ClF signals. However, the results are interesting in themselves and deserve further consideration. The assignment to Cl_2 was checked by growing samples from pure Cl_2 reservoirs.

6.4.1 B state excitation

Fig 6.15 collects the spectra recorded for Cl_2/Ar with LIF detection at 360 nm, indicative of Cl^+Cl^-/Ar fluorescence (Fig. 4.8). The pump wavelength is fixed at $\lambda_{pump} = 387$ nm and the

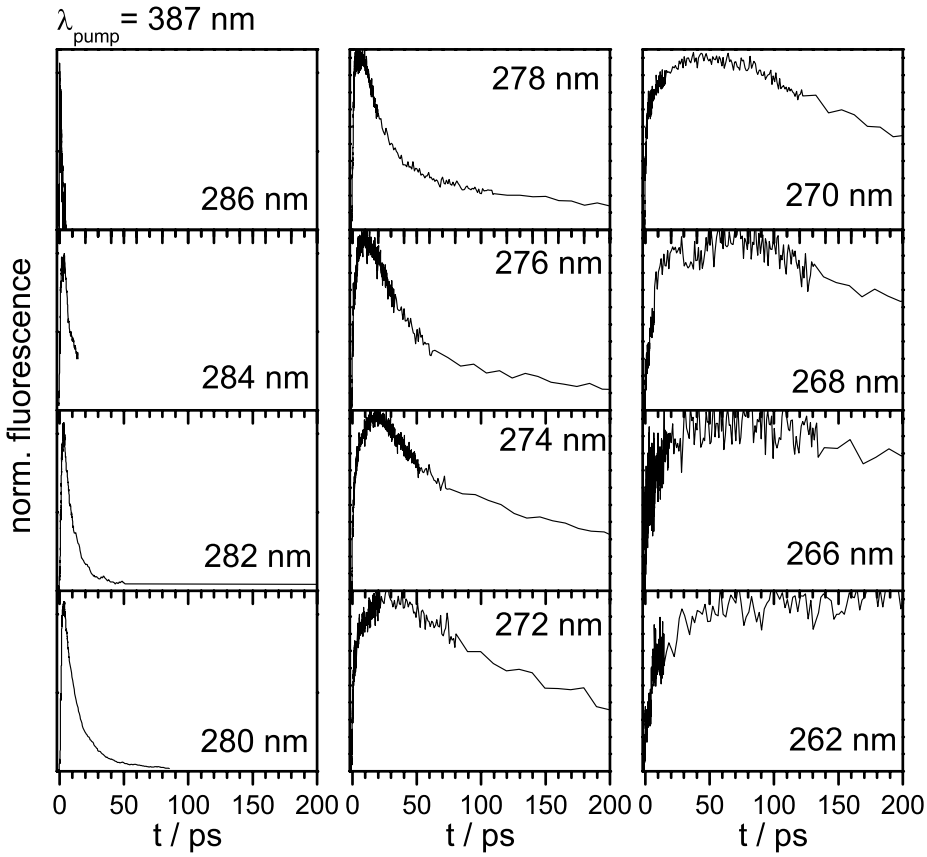

Figure 6.15: Pump-probe spectra with $\lambda_{pump} = 387$ nm. λ_{probe} is varied from 286 to 262 nm. The fluorescence is detected at $\lambda_{LIF} = 360$ nm and therefore only Cl_2 population is observed (see the fluorescence spectra in Fig 4.8). The maxima of the pump-probe envelope correspond to the delay time τ_m at which the vibrational population passes E_{win} (see Fig. 7.13). The early maxima in the first column are identical to those shown in the last column in Fig. 6.8, marked with an asterisk.

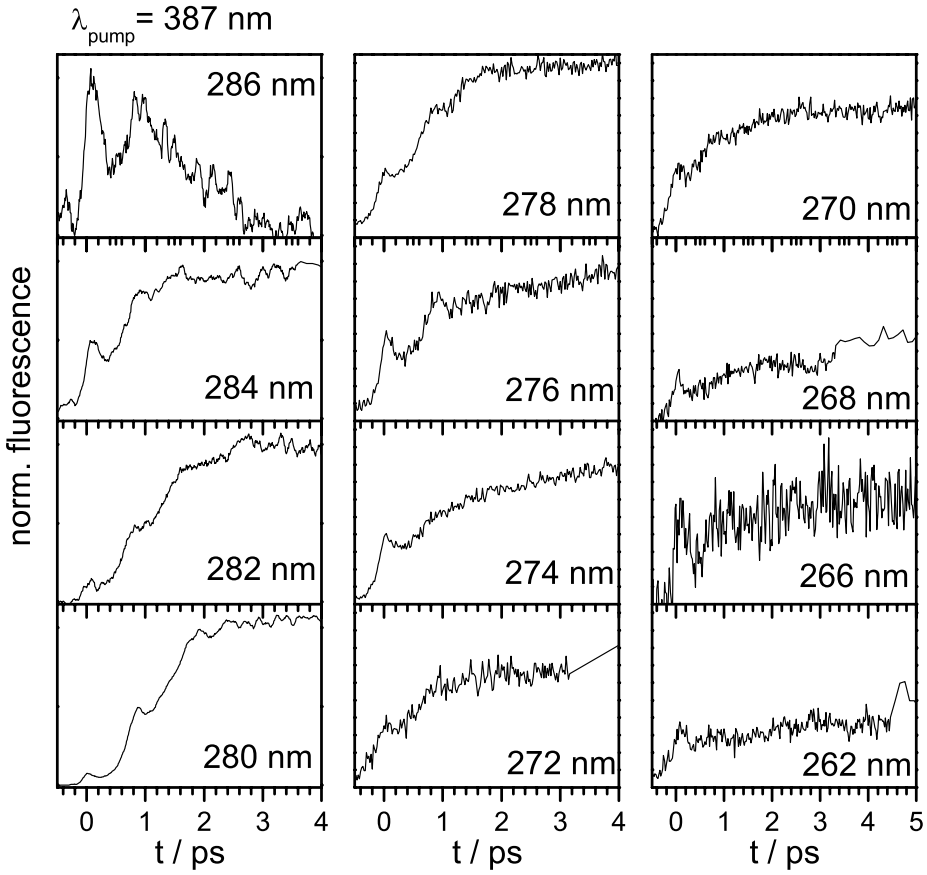

Figure 6.16: Pump-probe spectra Fig. 6.15 on a shorter timescale where $\lambda_{pump} = 387$ nm. λ_{probe} is varied from 286 to 262 nm. The fluorescence is detected at $\lambda_{LIF} = 360$ nm and therefore only Cl_2 population is observed (cf. Fig 4.8).

probe pulse is tuned from $\lambda_{probe} = 286$ to 262 nm. The first column shows spectra for $\lambda_{probe} = 286$, 284 and 282 nm, which have the same pump and probe wavelengths as the last column in Fig. 6.8 but there the LIF was detected at 420 nm, where both Cl^+Cl^-/Ar and Cl^+F^-/Ar emit (see the fluorescence spectra in Fig. 4.8). Therefore these spectra have an early, sharp maximum at $t < 5$ ps, marked with an asterisk (*) in Fig. 6.8, due to Cl_2 and a late maximum ($t > 40$ ps) due to ClF.

In pure Cl_2/Ar samples, identical results are obtained for $\lambda_{LIF} = 360$ nm (Cl^+Cl^-/Ar). However, for $\lambda_{LIF} = 420$ nm only the early peaks due to Cl_2, marked with an asterisk (*) persist, while the late maxima due to ClF are missing in Fig. 6.15. This substantiates the assignment of the 360 nm emission to Cl_2. For probe wavelengths $\lambda_{probe} > 290$ nm, the 420 nm emission is exclusively from ClF, and for shorter wavelengths due to both species. The different temporal shape of the Cl_2 vs. ClF dynamics is exploited for a two-pulse control scenario in chapter 7.8.

Fig 6.16 reproduce the spectra from Fig. 6.15 on an shorter time scale to display the wave packet dynamics. All spectra show an oscillatory period of approx. 800 fs. In some spectra an additional splitting of 150 - 200 fs is observed.

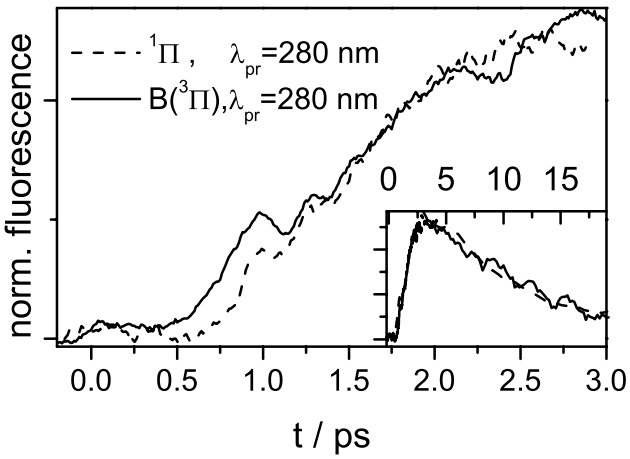

Figure 6.17: Comparison of fs-pump-probe spectra with $\lambda_{pump} = 387$ nm ($B(^3\Pi_0)$ excitation) and 290 nm ($^1\Pi_1$ excitation) with fixed $\lambda_{probe} = 280$ nm. The fluorescence is detected at $\lambda_{LIF} = 360$ nm and thus only Cl_2 population is observed (cf. Fig 4.8).

6.4.2 $^1\Pi$ state excitation

As in ClF and I_2, the excitation of Cl_2/Ar to its repulsive $^1\Pi_1$ states yields almost identical dynamics as excitation to $^3\Pi_0$. This is demonstrated in Fig. 6.17, which shows fs-pump-probe spectra with $\lambda_{pump} = 387$ and 290 nm and fixed $\lambda_{probe} = 280$ nm. The fluorescence is detected at $\lambda_{LIF} = 360$ nm and therefore only Cl_2 population is observed (cf. Fig 4.8). The assignment of these dynamics was tested by preparation of pure Cl_2/Ar samples without ClF impurities. The potential surfaces of Cl_2/Ar (cf. Fig. 5.7) are very similar to those of ClF/Ar. Transitions from the bound triplet states $^3\Pi$ are - analog to the discussion for ClF - the only candidates for the observed probe transition. Obviously, the wave packet nonadiabatically passes from the excited singlet state to a lower and bound triplet state in the first ps.